Figure 16

Simulated (symbols) and observed (curves) vertical distribution of salinity and temperature along transect A on four days during the synoptic survey.

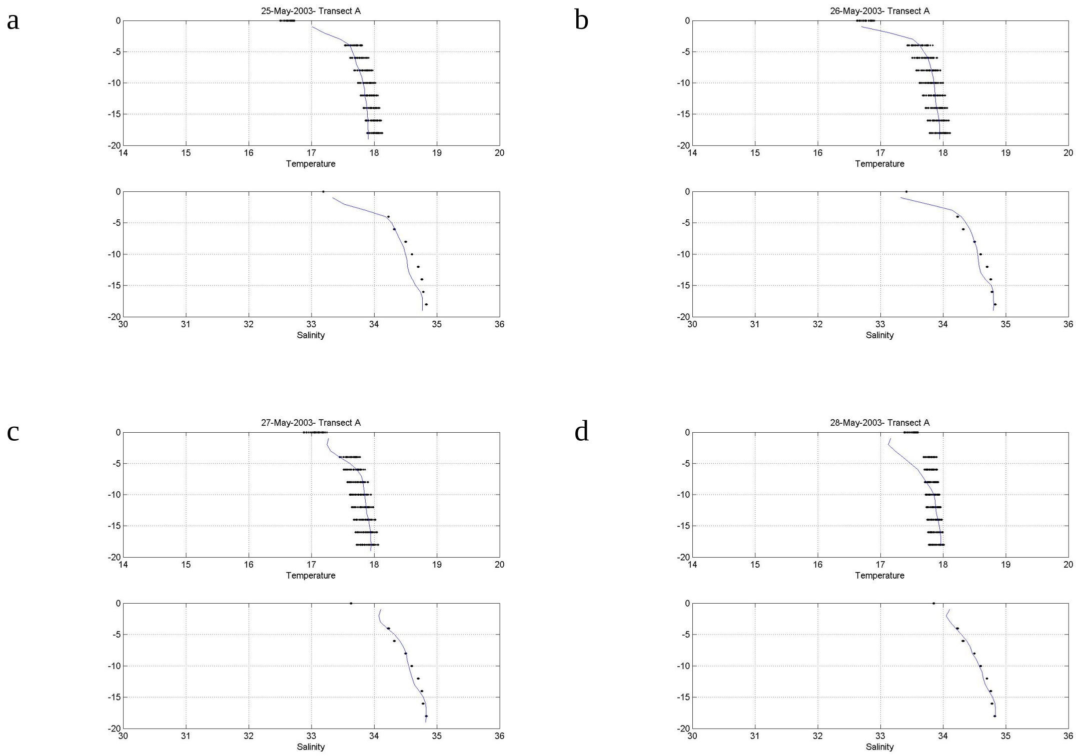

6 Results (Biophysical & logistic models)

Within this section we describe the results stemming from application of the biological models (in the form that they were used in the scenario simulations described in Broekhuizen et al. (2004), and driven by the hydrodynamic model as parameterised for the simulations listed in Broekhuizen et al. (2004)).

6.1 Biophysical Model

6.1.1 Temporal changes

Figure 17 presents the time-series of simulated, firth-wide average phytoplankton abundance. The model correctly reproduces the increase in diatom abundance and the decline in dinoflagellate abundance. Whilst the field-data indicate that phytoflagellate abundance remained approximately constant through May in the Wilson Bay area, the model suggests a steady decline in Firth-wide abundance. The Firth-wide total chlorophyll concentration (inferred from the simulated taxon-specific carbon concentrations and fixed, taxon-specific C:chl ratios) is predicted to have declined by ~15% over the duration of the study period. The Group A field-data indicate, that in the region of Wilson Bay, chlorophyll concentration rose slowly over this period.

Table 1 and Table 2 summarise the results from the virtual-sampling data. The daily average simulated chlorophyll is invariably below the corresponding average in the field-data, but on each of the five days the simulated sample average is not significantly different from the sample mean of the field data (two-tailed t-test for comparison of sample means, $P>0.05$). Sample mean simulated DIN concentrations are also below the observed field averages on all five days, but are not significantly different from the field sample means on three of the five days (two-tailed t-test for comparison of sample means, $P>0.05$).

The coefficients of variation (CV=standard deviation/mean, not shown) associated with the daily estimates of average biomass (stemming from the 49 station sampling) for simulated chlorophyll are approximately three times larger than those in the field-data; those for simulated DIN are approximately twice the ones derived from the field-data. Clearly, the biophysical model is predicting greater spatial variability than was evident in the field at the time of the synoptic survey. In the case of the chlorophyll, this is largely because the chlorophyll concentrations inferred from the model exhibit an overly large onshore/offshore concentration decline relative to the decline evident in the field data (Figure 18 a & b); however, in contrast to our assumption, Chl:C ratios inferred from the field data show some evidence of being greater nearshore than offshore (Figure 18c). Thus, in part at least, the overly-large onshore/offshore gradient exhibited by the inferred chlorophyll appears to reflect a failure to properly account for spatial structure in carbon:chl ratios when inferring simulated chlorophyll from simulated carbon. We have chosen not to endeavour to correct for the C:chl ratio-gradient evident in the field data for two reasons: (i) we have data only for a sub-sample of the 49 stations, and, for these, only on the first and last day of the survey, (ii) to maintain full independence between simulations and data.

Figure 17

Time-series of domain-wide simulated phytoplankton carbon-concentration (as diatom (solid line), phytoflagellate (dashed line) and dinoflagellate (dotted line), upper panel) and as chlorophyll (lower panel). In the lower panel, we also illustrate the inferred chlorophyll concentrations (circles) derived from the simulated carbon abundance at each of the 49 stations of the synoptic survey grid on each of the five days of the synoptic survey. Simulated concentrations during the first eight days of the simulation have been masked.

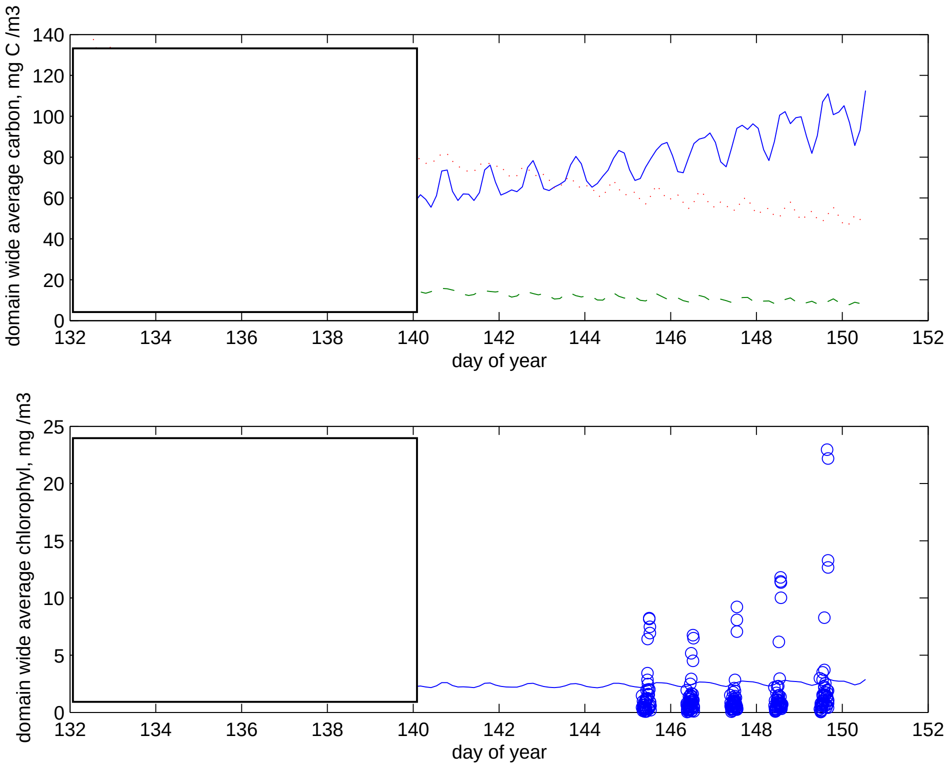

Figure 18

Bubbleplots of (a) observed chlorophyll abundance, (b) simulated chlorophyll abundance, (c) the ratio of simulated abundance to observed and (d) chl to carbon ratios (from the field-data) at stations 1, 5 and 7 of each of the seven inshore/offshore sampling transects. In (a) and (b) the five rows of images correspond to the five consecutive days of the survey. In (d) the upper figure is for the first day of the survey, and the lower figure is for the last day. Within each column of figures all bubbles were drawn to the same scale; the scales in (a) and (b) are the same.

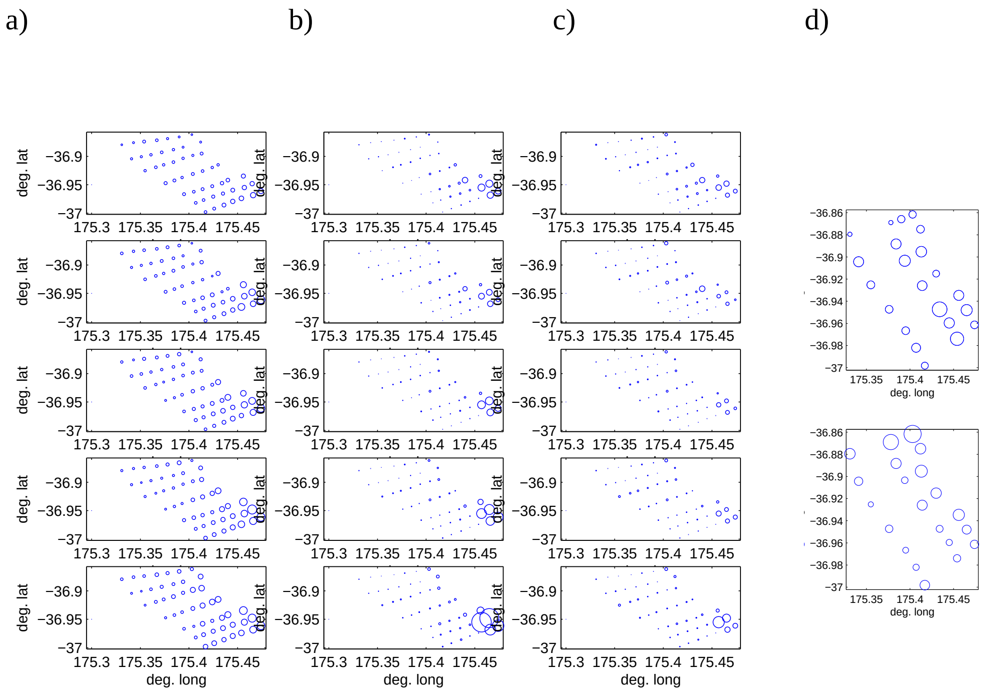

Table 1

Summary statistics for simulated chlorophyll concentrations (mg Chl a m^{-3}) inferred from the virtual sampling data. The statistics were derived from the entire 49 stations' worth of data on each day. The simulated mean is deemed to match the field-estimate if the corresponding simulation and field sample means cannot be distinguished statistically (2 tailed t-test, P>0.05).

	Day 1	Day 2	Day 3	Day 4	Day 5
Simulated mean matches field mean	Yes	Yes	Yes	Yes	Yes
Median	0.85	0.77	0.72	0.71	1.12
Std. Dev	2.15	1.70	2.19	2.98	4.92
Max	8.24	6.76	9.22	11.80	22.96
Min	0.07	0.04	0.06	0.08	0.04

Table 2

Summary of statistics for simulated dissolved inorganic nitrogen concentrations (mg N m^{-3}) inferred from the virtual sampling data. The statistics were derived from the entire 49 stations' worth of data on each day. The simulated mean is deemed to match the field-estimate if the corresponding simulation and field sample means cannot be distinguished statistically (t-test, P>0.05).

	Day 1	Day 2	Day 3	Day 4	Day 5
Simulated mean matches field mean	No	Yes	Yes	Yes	No
Median	6.62	7.03	7.37	8.44	9.02
Std. Dev	6.31	6.36	6.32	6.06	6.20
Max	30.07	32.50	34.92	39.26	40.93
Min	0.37	0.69	0.93	1.18	2.56

6.1.2 Comparison of depletion inferred from the field data and that inferred from the difference between no-farms and with-farms simulations

One means of estimating farm-induced depletion from our simulation results is by comparison of the results of the with-farms and no-farms simulations. This can be made for either: (a) time-averaged results, or (b) results from the virtual sampling.

We start by presenting a comparison of time-averaged results with and without farms (Figure 19). Dissolved inorganic nitrogen is predicted to be most abundant to the SE of Wilson Bay. From an initially homogenous spatial distribution, the phytoplankton evolve marked concentration gradients – being generally more abundant on the eastern side of the Firth.

Though somewhat masked in the simulation-derived time-averages, comparison of the 0-18 d time averages with 13-18 d ones provides indications of the aforementioned differential changes in the abundance of the three phytoplankton taxa. Both the 0-18 d time average and the 13-18 d time averages predict that chlorophyll depletion (<10%) occurred around the NE region of Wilson Bay Area A. The location of this depletion is in accord with that inferred from the field-data; the magnitude of depletion is lower than inferred from the field data. On a less satisfactory note, we remark upon the predicted 'enhancement/depletion spiral' to the SW of Area A. This was not observed in the field data. The field data did show elevated absolute chlorophyll concentrations inshore relative to offshore, but this was assumed to be a 'natural' phenomenon, rather than being farm-induced. The no-farms simulation reproduces the onshore elevated chlorophyll concentrations, but this enhancement is still greater in the with-farms simulation (Figure 19). As with the enhancement/depletion spiral, we believe that this is probably also an erroneous prediction.

As well as comparing time-average results, we can also compare the chlorophyll concentrations inferred from virtual synoptic surveys run within the no-farms and with-farms simulations (Figure 20 and Table 3). On a day-by-day basis, the station-specific simulated concentration-ratios (1+(with farms-nofarms)/no farms) are variable, but all indicate enhancement *cf* the depletion that was inferred from the field data.

Table 3

Mean and median change inferred from a comparison of biophysical model results the with-farms and no-farms virtual sampling data. Statistics are derived from all 49 stations. The 5-day average ratios are ratios of the 5-day average biomasses rather than simple averages of the five, daily ratios). Values<1.0 indicate depletion; values >1.0 indicate enhancement.

	Day 1	Day 2	Day 3	Day 4	Day 5	Day 1-Day 5
Mean	1.11	1.08	1.15	1.13	1.12	1.08
Median	1.07	1.00	1.03	1.09	1.11	1.03

Figure 19

Time and depth-averaged simulated concentrations of DIN (mg N m-3), diatom, phytoflagellate and dinoflagellate abundance (mg C m-3) and inferred chlorophyll a (image columns 1 and 3) in the Wilson Bay area under a no farm scenario. Image columns 2 & 4 illustrate the 'with-farms' time-and-depth-averaged concentrations relative to those of the 'no-farms' situation. Areas of blue colour indicate 'low' values (be they concentration or concentration ratios). Areas of red indicate 'high' values. The colour-scales are indicative of $\log_{10}$(concentration) or $\log_{10}$(concentration ratio). The locations of the 3 farm areas are indicated by black polygons in the ratio plots. The survey grid employed by Gall et al. (2003) spanned a large fraction of the area of each image. Image columns 1 & 2 present averages over the entire duration of the simulation. Image columns 3 & 4 present averages over the period corresponding to the field-survey. Each small pixel corresponds to an area of 750 m x 750 m.

Property	Time-averaged results (13-30 May)		Time-averaged results (25-30 May)	
	Concentration	concentration ratio	concentration	concentration ratio

DIN (mg C m^{-3})

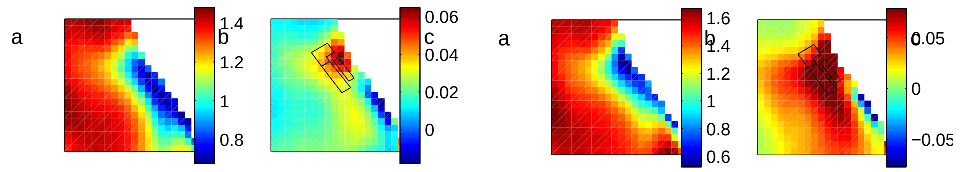

Diatom C (mg C m^{-3})

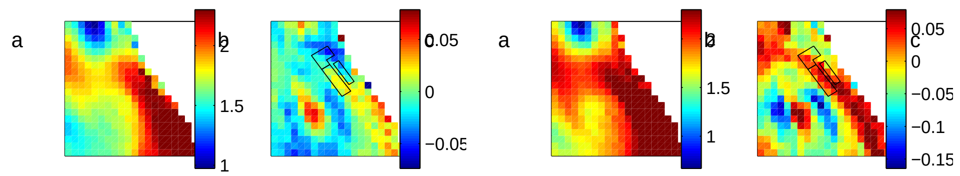

Phytofl. C (mg C m^{-3})

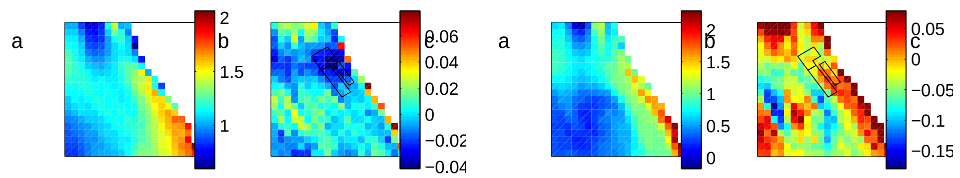

Dinofl. C (mg C m^{-3})

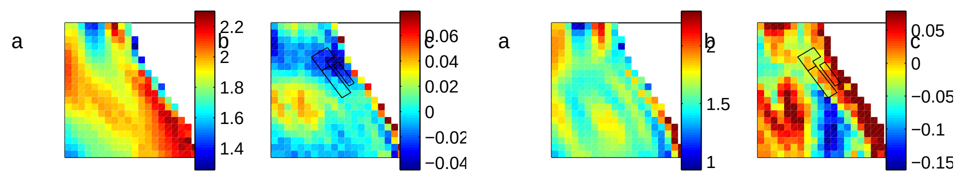

Inferred chlorophyll a (mg m^{-3})

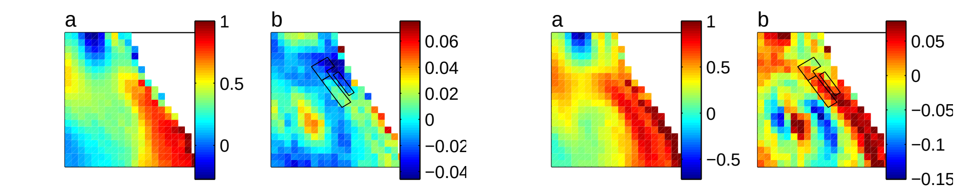

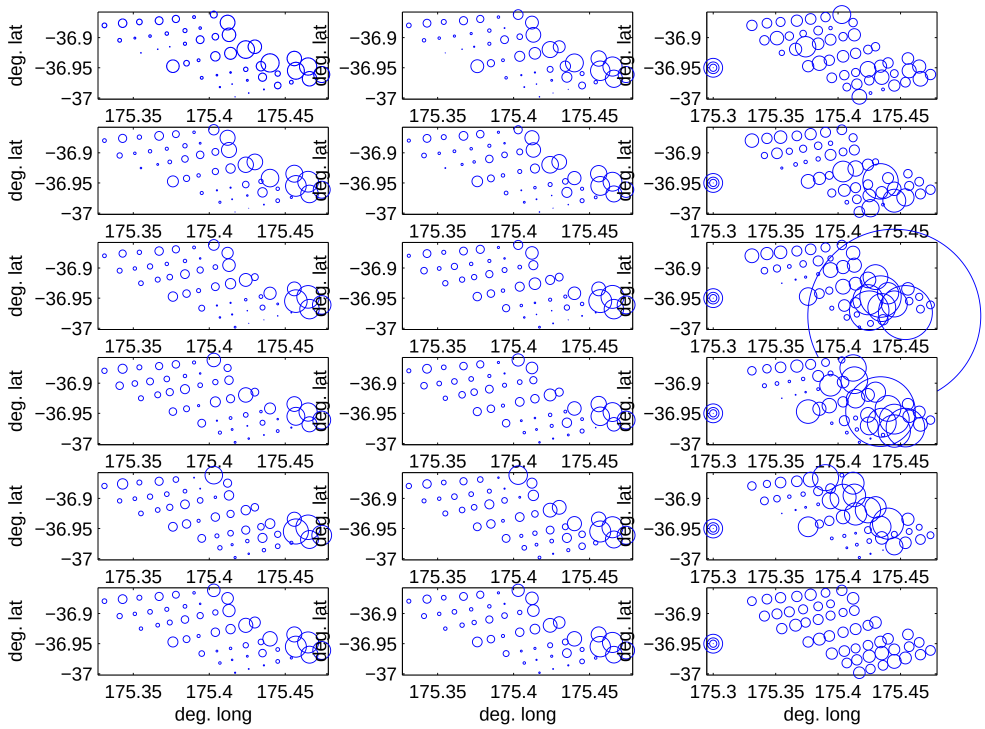

Figure 20

Bubbleplots illustrating the biophysical-model simulated station-specific relative concentrations of chlorophyll (-) at the 49 stations on the five days of virtual sampling (upper five rows; the lower-most row presents the five-day average results). Left column: 'no farms' simulation, centre column 'with farms' simulation, right column is the concentration ratio 'with farms/no farms'. Circle diameters are indicative of log(1+concentration), or of the ratio. The concentric circles on the left-hand edge of the ratio plots correspond to ratios of 0.0, 1.0 2.0 and 5.0.

6.1.3 Comparison of depletion inferred from the field data and the simulated data using the surfaces method

We have established that the biophysical model reproduces temporal trends of DIN, total algal biomass, and phytoplankton taxonomic composition moderately well. By means of comparison of the time-averaged results (*cf* virtual sampling results) from a no-farms and a with-farms simulation, we have also established that it indicates depletion around the north of Area A – as inferred from the field data. Equally, however, it is indicating inshore enhancement, and some near-field change to the SW of the farmed area that was not revealed by the surfaces method that Gall et al. applied to the synoptic survey field data.

Whilst the simulation results clearly have some errors, they agree with the field data in: (a) temporal trend and area-average biomass, (b) time-average location of depletion. This level of agreement between model results and inferences drawn from the field data is encouraging, but our conclusions related to depletion can be criticised on the grounds that we are not comparing 'like-with-like'. We have inferred depletion from a comparison of no-farms and with-farms simulation results and then compared the results with the results derived from the surfaces method applied to the field data. It can be argued that we should instead compare the results of the surfaces method applied to both the field-data and our with-farms simulation results.

Unfortunately, there are strong reasons to support an *a-priori* belief that the surfaces method will not perform well when applied to our simulated data. In contrast to the pattern evident in the field data, the model predicts an overly strong onshore/offshore decline in phytoplankton abundance – in both the no-farms and the with-farms simulations (Figure 18 & Figure 20). Furthermore, this trend in abundance is step-like, rather than smooth: biomasses in the inshore-most two rows of stations are markedly too high, whilst those in the remaining transects are markedly too low. The surfaces method infers farm influence by: (i) fitting a surface through data stemming from all stations, and a second surface through data stemming from those stations somewhat beyond the farm's perimeter, and then (ii) attributing any differences between the two surfaces to the influence of the farm. This method becomes progressively less robust as the spatial gradients of biomass become more variable (Figure 21 and associated legend). Our simulated data have a structure close to that of Figure 21b, whilst the field data have a structure more like that of Figure 21a. Thus, we anticipate that whilst the surfaces method has probably yielded robust results when applied to the field data, it is likely to yield deceptive results when applied to our simulated data.

Figure 21

Schematised illustration of the surfaces method applied to artificial data having (a) smoothly varying and (b) rapidly varying spatial gradients. The pink and blue symbols denote the (artificial) data. The blue curves are least-squares best-fit quadratic curve fitted to all of the data (blue + pink symbols). The pink curve is the least-squares best fit curve fitted to a subset of the data (pink symbols only). Consider a situation in which no farm is present, and the spatial variation in biomass is therefore 'intrinsic' (has nothing to do with the presence/absence of a farm). Now let us choose to drop the point corresponding to x=3 (as though a farm occupied this site). In (a) the curve fitted through all the data, and the curve fitted through all the data except that from x=3 are very similar. The method allows us to conclude correctly that our (entirely imaginary) farm has no significant impact. In (b) the two curves are very different and we falsely conclude that our (entirely imaginary) farm is having a substantial impact.

a)

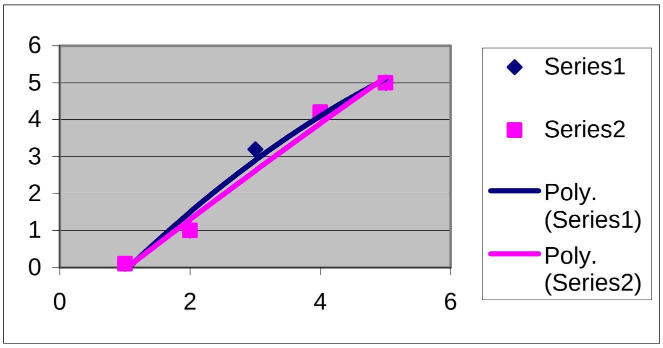

b)

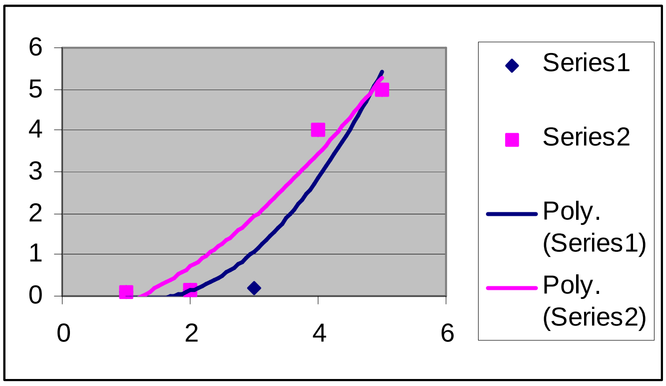

To determine whether or not the surfaces method might yield robust results when applied to our with farms simulation results, we first apply it to the no-farms results – but calculating S_{out} by excluding those stations which would be excluded if the Wilson Bay farms had been present in the simulation. Since there were no farms in the simulation, the method should indicate 'no change'; instead, it gives a false indication of change (results not shown). This is due to the high station-to-station variations in abundance predicted by the model. Thus, we cannot hope to derive robust results by applying the surfaces method to our 'with-farms' simulation results and we do not proceed with that analysis.

6.2 Empirical model

Figure 22 illustrates the time-and-depth averaged abundances of each of the sub-classes in the empirical model, along with the time-averaged depletion ratios. The analogy between the model's five sub-classes of logistically growing plankton and the phytoplankton sampled within the field is much more tenuous than that which holds for the biophysical model. The empirical model does not have a mechanistic description of plankton growth. Rather, it aims to reproduce a plausible range of planktonic growth rates. The first three sub-classes have relative vulnerabilities to consumption by mussels of 1.0 – consistent with them being representative of phytoplankton. Sub-classes four and five have vulnerabilities of 0.3 and 0.2 respectively – rendering them more analogous to meso-zooplankton. Respectively, the first three sub-classes have maximum weight-specific growth rates of 2.0, 1.0 and 0.2 d^{-1}. All are higher than that inferred from the field data (calculated to be <0.1 d^{-1} assuming that the net change in observed chlorophyll biomass over the course of the synoptic survey was due solely to cellular growth, rather than net immigration, changes in cellular chlorophyll content or changes in weight-specific mortality rates). We adopt sub-class three as being the closest analogue to the population of phytoplankton that was present during the synoptic survey.

In addition to the maximum growth rate- and relative vulnerability parameters, the logistic growth equation that our plankton model is based upon has a third sub-class-specific parameter: the local (in space) carrying capacity. This defines the ultimate concentration to which the sub-class would evolve were it not continually subjected to disruption by current-driven immigration / emigration and (at some locations) mussel-induced mortality. The speed with which the population moves towards its local carrying capacity is determined by the maximum growth rate parameter. For the purposes of this verification exercise, we were required to retain the parameters that were used in our earlier scenario-simulations (Broekhuizen, N. et al. 2004). In those simulations, we chose to assume that the carrying capacity varied across space in a bivariate-normal manner, with the spatial maximum being located in the northern central firth. Comparison of the biomass distributions of the five plankton sub-classes (Figure 22) provides some indication of the manner in which current-driven transport and (to a much lesser extent) farms induce deviations for the bivariate normal spatial pattern. Though less evident in these local-to-Wilson Bay plots, plots showing the firth-wide biomass-distribution (not shown) reveal a second feature: in areas where the depth-integrated abundance of plankton is lower (either because the plankton concentration is low, or because the water is shallow), the ratio of with-farms simulated concentration to without-farms simulated concentration tends to be more variable across adjacent 750 x 750 m water-columns, and to deviate further from 1.0. Broekhuizen et al. (2004) provide an explanation for this pattern. It stems from an important characteristic of the particle-tracking approach: namely that the accuracy with which local abundance can be resolved is inversely related to the number of particles within the volume over which the average is being determined (see section 7.2). In effect, 'sampling error' becomes large where there are few particles (in shallow water, and where population abundance is low). By examining long-term averages, one increases the number of particles contributing to the estimate of abundance – thereby improving the resolution and generating more robust results. This is why the 18 d time-averaged ratios are less variable across space, and deviate from 1.0 to a lesser degree than the 5 d ones. As we will see, the estimates stemming from the (near) instantaneous virtual sampling designed to mimic the synoptic survey exhibit still greater variability.

The chlorophyll concentrations inferred from model sub-class three (our chosen analogue to the community of phytoplankton in the vicinity of Wilson Bay at the time of the survey) in the vicinity of Area A are below those measured during the synoptic survey. Nonetheless, this should not be taken as evidence that the model is fundamentally in error. Local abundance is very strongly influenced by the local carrying capacity. This is specified a-priori. For the purposes of this verification exercise, we were required to retain the model formulations and parameterisations used in the scenario simulations (Broekhuizen, N. et al. 2004). The parameterisation defining this spatial pattern was chosen to be consistent (in a very general sense) with data gathered over the summers of 1985-1987. Chlorophyll concentrations measured in the northern Firth during that period were usually rather lower than those inferred from measured fluorescence at NIWA's Firth of Thames mooring site during the period of the synoptic survey. Thus, it is no surprise to find that chlorophyll abundance inferred from the simulation results is somewhat below that measured (this remains true, even if one infers chlorophyll abundance from the sum of the simulated abundances of the first three simulated phytoplankton-like sub-classes). Given that local abundance is determined not only by the prescribed carrying-capacity, but also by water-transport and mussel-feeding (the former being an emergent property of the hydrodynamic model, the latter being an emergent property of the biological models), the model's under-prediction of chlorophyll provides (weak) evidence that it is performing in a plausible manner.

Table 4 presents a summary of the virtual-sampling results for plankton sub-class three in the with-farms simulation. Average and median concentrations change little over the period of the survey. The coefficients of variation are substantially smaller than those derived from the results of the biophysical model. Nonetheless, they remain somewhat higher than those estimated from the field measurements of chlorophyll concentration.

In contrast to the biophysical model results, there is no evidence for a marked onshore/offshore gradient across Area A in the simulation data (Figure 22) – probably reflecting the comparatively shallow slope of the prescribed gradient in the carrying capacity function in this region. Whilst it may merely be a fortuitous result driven by the shape of the underlying, prescribed carrying capacity, it is encouraging to note that the model is reproducing the area of high chlorophyll concentration towards the SE of Area A that was detected in the field data.